Macromolecules
ARTICLE

Macromolecules **2011**, *44*, 913–922 **913**
DOI: 10.1021/ma102486x

Low-Field NMR Investigations of Nanocomposites: Polymer Dynamics and Network Effects

Aurélie Papon,[†] Kay Saalwächter,*[,‡] Kerstin Schäler,[‡] Laurent Guy,[§] François Lequeux,[†] and Hélène Montes*[,†]

[†]*PPMD-SIMM, Soft Matter Science and Engineering, UMR 7615 CNRS/UPMC/ESPCI ParisTech, 10 rue Vauquelin, F-75231, Paris Cedex 5, France,* [‡]*Institut für Physik−NMR, Martin-Luther-Universität Halle-Wittenberg, Betty-Heimann-Strasse 7, D-06120 Halle, Germany, and* [§]*Rhodia Opérations, 15 rue Pierre Pays, BP 52, F-69660 Collonges-au-Mont-d'Or, France*

Received November 5, 2010; Revised Manuscript Received January 4, 2011

ABSTRACT: The dynamics of the polymer matrix in filled rubbers is modified by the presence of solid particles. We used low-field proton NMR to investigate model filled samples consisting of a dispersion of grafted silica particles into an elastomeric matrix. Exploiting magic-sandwich echo experiments, we were able to determine the fraction of polymer with slower dynamics and to correlate it to the silica specific surface. The presence of immobilized polymer—most probably due to a gradient of glass transition temperature around the solid particles—is detected whether there is a covalent bond between the filler and the matrix or not. Moreover, the fraction of immobilized polymer decreases in similar ways with either an increase of the temperature or the addition of solvent. In the case of covalent bonds between the silica and the polymer, multiple-quantum experiments reveal that the cross-link density of the elastomer matrix is locally increased in the vicinity of the particles. This is an observation that was not made in any conventional filled elastomer system and it can be attributed to the good particle dispersion and the covalent links in our model samples.

Introduction

It is a very standard procedure to introduce solid fillers in a rubbery matrix in order to improve its mechanical properties. It leads to an increase in the elastic modulus, fracture, and abrasion resistance. However, this improvement is not a simple geometrical effect due to the presence of a solid fraction in the polymer, but a consequence of the modification of the polymer dynamics near the interface with the fillers.[1−4]

The study of the polymer mobility in filled rubbers is thus of great importance and low-field proton NMR is a very well established method for this purpose. T_2 relaxometry has already permitted to distinguish between different polymer mobilities in filled rubbers and the presence of a layer of immobilized polymer of a few nanometers around the fillers has been detected in several systems.[5−10]

The modification of the polymer dynamics near a solid surface has also been evidenced on thin polymer films deposited onto substrates.[11] In the case of strong interactions between the polymer and the substrate such as hydrogen bonds, the glass transition temperature has been shown to increase when the polymer film thickness decreases. This behavior can be described by a gradient of glass transition temperature near solid surfaces:[12]

$$T_g^f(z) = T_g^f(1+(\delta/z)^v) \quad (1)$$

where $T_g^f(z)$ is the glass transition temperature of the polymer at a distance z from the substrate at the frequency f, T_g^f the glass transition temperature of the bulk polymer, δ a length related to the amplitude of the gradient and v an exponent close to 1. This model describes the presence of immobilized polymer in filled rubbers that has been experimentally measured with NMR experiments.[13−15]

We also pointed out that the mechanical nonlinearity usually observed in filled rubber—known as Payne effect—is related to the stress-softening of the polymer glassy bridges between neighboring particles.[16] A better understanding of the polymer mobility around the fillers is thus of great importance since the presence of an immobilized polymer layer around the silica particles and the potential formation of glassy bridges between the particles govern the mechanical behavior of the filled samples.

The NMR sequences generally used to study polymer mobility in filled rubbers are the solid-echo pulse sequence to study the rigid polymer fraction (seen at short time scales) and the Hahn echo for the mobile fraction (at longer time scales). However, those methods are potentially subject to artifacts related to overinterpreted or inapplicable fitting models and parameter interdependencies.[17,18] That is why we propose here to use two more reliable techniques.

On the one hand, we use magic-sandwich echo (MSE) to study the polymer relaxation at short time scales (less than 0.2 ms). The MSE refocuses the initial part of the free-induction decay (FID) and thus avoids the dead time issue. Compared with solid echo, it enables a better refocusing of multispin dipolar interactions and has been shown to be a robust method to investigate polymer mobility.[19,20] On the other hand, multiple-quantum (MQ) experiments give access to much slower relaxation processes (0.1−3 ms), which are linked to the presence of topological constraints such as cross-links and/or entanglements that are limiting the reorientations of the polymer segments. This method is more quantitative than T_2 relaxometry since it measures the residual dipolar coupling and thus the local dynamic order parameter on an absolute scale.[17,21−24] These two complementary methods give us a broader view on the polymer dynamics in filled elastomers: the MSE enables the study of the polymer mobility and the

*To whom correspondence should be addressed. E-mail: (K.S.) kay.saalwaechter@physik.uni-halle.de; (H.M.) helene.montes@espci.fr.

Published on Web 01/21/2011

determination of the immobilized polymer fraction, while MQ NMR gives us an insight into the cross-link density and homogeneity in the filled samples.

Another critical parameter in the study of the polymer dynamics in filled rubbers is the control of the dispersion of the fillers in the samples. In effect, if the polymer mobility is influenced by the presence of solid surface, it is then crucial to control the quantity of silica surface accessible to the polymer and thus the dispersion state of the fillers. This is why this study was conducted on model-filled samples with a much better controlled dispersion state than in conventional samples. We varied both the silica content and the particles diameter. Moreover, using two different synthesis methods, we were able to make filled samples with two kinds of "coupling" agents—the molecule coating the silica surface: one creating a covalent bond between the silica and the polymer, and the other just modifying the surface energy. In the latter case, the interaction between the filler and the matrix is mainly governed by hydrogen bonds between residual silica OH groups and the polymer chains. We could thus study the influence of the coupling agent on the polymer dynamics.

Model samples with a grafter creating a covalent bond between the silica and the polymer have already been studied in NMR and the presence of glassy polymer has been detected.[13−15] Here, the analysis of MSE-refocused FIDs will give a more precise description of the polymer dynamics near the interface which is in agreement with the presence of a *gradient* of mobility that cannot be described with a core−shell approximation at low temperature. Moreover, with this method the presence of polymer with a slower dynamics could also be detected in samples with a weaker coupling between the silica and the polymer (hydrogen bonds). The relaxation of the polymer at long time scales has also been examined in a previous publication[25] with the study of Hahn or pseudosolid spin−echoes. This analysis revealed an increase in the overall effective cross-link density compared to the amount of cross-linker introduced. It showed that the presence of solid particles plays a role in the effective cross-link density of filled rubbers. This result is now clarified by our MQ NMR measurements. In effect, we show here that if most of the elastomer has a slightly higher cross-link density than the reference matrix, a fraction of up to 30% of the polymer—most probably in the vicinity of the solid particles—has a far larger cross-link density. This effect had not been previously seen in conventional samples and is probably due to the good silica dispersion in those model samples.

In this paper, we will first describe the sample preparation and the two NMR methods used. We will then expose the experimental results obtained from (MSE-refocused) FIDs and MQ NMR. For each method, we will start with the study of the elastomer matrix before investigating the model filled samples. Finally, we will discuss the role of the connection between the silica and the polymer on the polymer dynamics.

Samples and Experimental Techniques

Sample Preparation. The model filled elastomers consist of grafted silica particles dispersed in a poly(ethyl acrylate) matrix. Two kinds of grafters have been used: TPM (3-(trimethoxysilyl)-propyl methacrylate), which can react with the monomer and thus create a covalent bond with the matrix (covalently grafted samples, CG), and C8TES (*n*-octyltriethoxysilane) with which there are only weak bonds between the silica particle and the polymer (noncovalently grafted samples, NCG). The synthesis process has been described elsewhere,[26] and we will here recall the main steps.

First, weakly polydispersed silica particles were synthesized using the procedure described by Stöber.[27] Then, the filled elastomers were obtained following the process developed by Ford et al.[28−31] for the TPM-grafted samples, and a process adapted by Berriot et al. for the C8TES samples.[14] For that, the silica particles were directly grafted in a diluted Stöber solution (particle volume fraction of 2%) with an excess amount of TPM or C8TES. The quantity of grafted coupling agent was determined by elemental analysis and is shown in Table 1. Then, the TPM-grafted particles were transferred by dialysis to methanol and then, again by dialysis, to the acrylate monomer. Various concentrations of silica were obtained by diluting the concentrated solution obtained after dialysis (20% in volume) with acrylate monomer. Finally, a photosensitive initiator (Irgacure from Ciba, 0.1 wt % to the monomer) and a cross-linker (butanediol diacrylate, 0.3 mol % to the monomer) were added and polymerization and cross-linking occurred simultaneously under UV illumination. The process used for C8TES-grafted silica was slightly different due to depletion issues observed during the synthesis. In effect, the colloidal stability is more difficult to preserve in the case of this coupling agent which does not create a covalent link with the polymer. The C8TES-grafted silica beads were first transferred to methanol by dialysis and then the desired amount of monomer was added. This way, the solution was kept diluted (around 6% in volume) so that the colloidal stability could be maintained. Part of the solvent was then evaporated by distillation at 50 °C until a concentration of 20% in volume was reached. The polymerization (same initiator and cross-linker as previously) was done in presence of solvent in order to reduce the depletion issues.

Table 1. Sample Characteristics (NCG = Noncovalently Grafted, CG = Covalently Grafted)

name	mean silica diameter (nm)[a]	vol. fraction ϕ_{Si}	graft density (nm^{-2})[b]
T30-NCG-18%	26	0.10	2.0
T30-NCG-25%	26	0.15	2.0
T30-NCG-37%	26	0.23	2.0
T50-NCG-18%	42	0.10	1.5
T50-NCG-25%	42	0.15	1.5
T50-NCG-44%	42	0.29	1.5
T30-CG-20%	27	0.12	5.0
T30-CG-25%	27	0.16	5.0
T30-CG-30%	27	0.20	5.0
T50-CG-18%	42	0.11	3.2
T50-CG-25%	42	0.15	3.2
T50-CG-30%	42	0.22	3.2

[a] From SANS measurements. [b] From elemental analysis.

SANS Measurements. The silica particles dispersion state was characterized with Small Angle Neutron Scattering (SANS) experiments.[26] Diluted solutions of silica particles gave access to the form factors and the structure factor could then be deduced by dividing the measured scattered intensity by the form factor. The intensity of the structure factor at low wavevectors q gives important information on the large-scale arrangement of the silica particles in the samples. When the intensity is low in this regime, it means that the particles are very homogeneously distributed in the sample, otherwise, it shows the presence of aggregates. All the samples used here showed a rather good dispersion. The characteristics of the samples are presented in Table 1.

Low-Field NMR Measurements. The NMR measurements were performed on a Bruker Minispec mq20 at 20 MHz proton resonance frequency. The sample temperature was controlled with a BVT3000 heater working with air or nitrogen gas at low temperature. For the experiments in presence of solvent (dichloroethane and toluene), the solvent was added to the sample in a conventional NMR tube. To avoid evaporation, the tubes were flame-sealed after dipping in liquid nitrogen.

The minispec has typical $\pi/2$ pulse lengths of down to 2 μs (125 kHz nutation frequency), it shows a reliable phase cycling in $\pi/2$ steps with switching times in the 2 μs range, and has a minimum dwell time of 400 ns. It is thus very well adapted to solid-state pulse sequences. Each signal trace required 64 scans with around 1 s recycle delay (depending on the temperature).

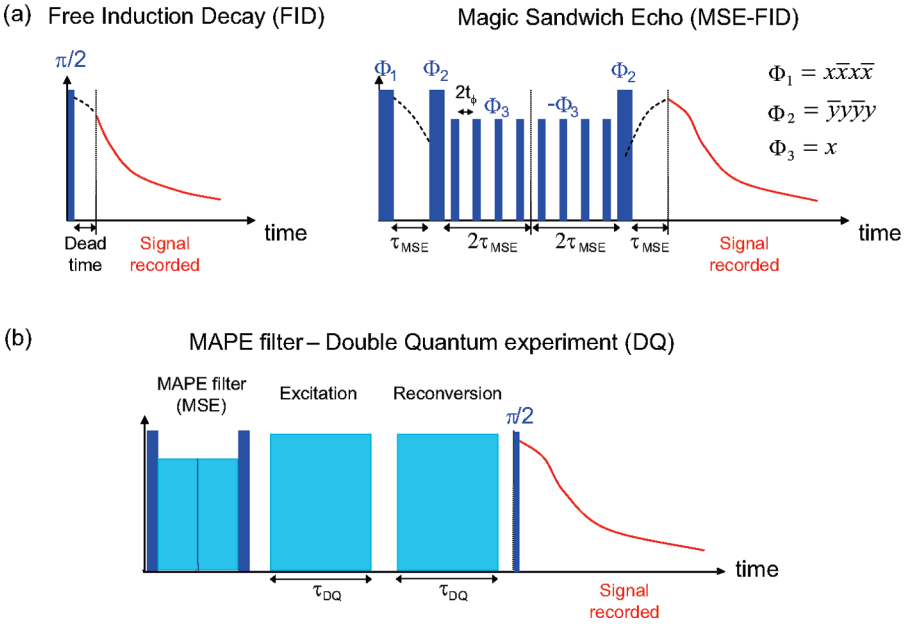

Figure 1. Pulse sequences. Solid bars denote 90° pulses, and the gray-shaded areas represent groups of pulses. (a) Initial part of the free-induction decay (FID) is missing due the dead time of the receiver. That is why we use the magic-sandwich echo (MSE) to refocus the signal and thus measure the entire shape of the decay. This sequence is used to study the polymer mobility in the filled samples. (b) Multiple-quantum (MQ) experiment (see ref 23 for details) is preceded by a MAPE filter (effectively an MSE sequence with longer interpulse spacings t_ϕ) in order to remove the response of the immobilized polymer fraction from the signal. This sequence enables the study of the topological constraints in the samples such as cross-links and entanglements.

Magic-Sandwich Echo. The rather long dead time of the low-field equipment (15 μs) is tackled by refocusing the free-induction decay (FID) signals with a magic-sandwich echoes (MSE) pulse sequence. This sequence is much more efficient than the conventionally used solid-echo, which cannot properly refocus multispin dipolar interactions. The pulse sequence used is sketched in Figure 1a, and was designed to accommodate the finite phase switching time t_ϕ of the instrument. See refs 19 and 20 for details.

Multiple-Quantum NMR. The precise procedure used for multiple-quantum (MQ) NMR experiments has been published previously,[23] and we will here simply recall the principle of the measurement and the main steps of the analysis.

The orientation of the polymer segments in a network can be described by an orientation autocorrelation function which for our NMR observable is the one of the second Legendre polynomial P_2. This time-dependent function gives the probability for a segment in a certain orientation at a time t_1 to be again in the same orientation at another time t_2. At short time differences $t_2 - t_1$, the polymer segments quickly loose their orientational memory due to fast local fluctuations, and the autocorrelation function decreases rapidly. At some point, however, the longer-range or slower motions of the segments are hindered by the presence of topological constraints such as entanglements and cross-links. This leads to a very slowly decaying component in the autocorrelation function, which can almost be seen as a plateau. In this case the height of the plateau of the P_2 autocorrelation function corresponds to the square of a dynamic order parameter of the polymer backbone S_b.

The parameter S_b is directly proportional to the cross-link density and is thus characteristic of the network structure. It can be readily obtained by MQ experiments at temperatures far above T_g via the measurement of normalized double-quantum (DQ) build-up curves. (Higher-order MQ coherences do contribute to the signals at long times, but are negligible in the theoretical treatment.) The rise time of the DQ build-up curves depends on the residual dipolar coupling, which is proportional to S_b. The DQ build-up curves were measured at 393 K and normalized in order to remove any temperature-dependent relaxation effects. The pulse sequence duration τ_{DQ} was varied between 0.01 and 70 ms, and for each value, the intensities of the DQ build-up curve (I_{DQ}) and a reference decay curve (I_{ref}) were measured. The sum of the two components contains the full magnetization of the sample and is used to normalize, at each time τ_{DQ}, the DQ build-up curves: $I_{DQ}^{norm} = I_{DQ}/(I_{ref} + I_{DQ})$. I_{DQ}^{norm} is then independent of the time scale of fast segmental fluctuations leading to intensity decay at long times. Thus, the residual dipolar couplings that are representative of the network structure are reliably accessible.

In the case of our model filled samples, even if the MQ experiments were done at high temperature (393 K, that is T_g + 120 K), the filled rubbers still contained a fraction of rigid polymer. This immobilized polymer interferes with the early part of the build-up curves representing the mobile elastomer part, since at very short τ_{DQ}, also signals of rigid, strongly dipolar-coupled segments contribute to the DQ intensity. The used MQ pulse sequence is not very efficient for strongly dipolar-coupled systems due to the rather long cycle time, yet in order to completely remove such unwanted contributions, we used a MAPE (magic and polarization echo) as dipolar filter, which is addressed in more detail in ref 20. In essence, it is identical to the MSE sequence with exception of the last "sandwich" pulse, whose phase is opposite to the one of the first pulse. By increasing the overall cycle time of the central spin-lock part of the MSE sequence the echo becomes inefficient for strongly dipolar-coupled spins and their signal is correspondingly suppressed. A long echo duration τ_{MAPE} was realized by an increase of the interpulse spacing t_ϕ. The time τ_{MAPE} was adjusted so as to remove the rigid fraction for all the samples (0.164 ms). We will explain this point in more detail in the MQ NMR section. The polymer motion in the filled elastomers has thus been studied in the rubbery part of the sample. The pulse sequence used is schematically shown in Figure 1b.

Experimental Results

Polymer Mobility: FID and MSE Measurements. The polymer mobility can in principle be investigated by simply

studying the free-induction decay (FID) signal of the samples. A slow decay of the FID corresponds to the response of mobile polymer whereas a rapid decay shows the presence of less mobile polymer. However in our case the FID could not be directly exploited due to the rather long dead time of the receiver: the first 15 μs of the FID are missing and this part of the signal is very important since it contains the initial fast decay part and so the immobilized polymer response. To obtain information on the shape of the entire signal decay we thus referred to an echo in order to refocus the signal.

The FID after a short MSE sequence gives the entire shape of the decay and can generally be well fitted with a combination of stretched or compressed exponential (Weibullian) functions $e^{-(t/\tau)^b}$ (henceforth referred to as "modified" exponential). With $b = 2$, the function corresponds to a Gaussian decay which can be used to describe the behavior of a rigid polymer, whereas a simple or slightly stretched or compressed exponential ($b \approx 1$) will be able to describe a more mobile elastomer. The weight of each fit component gives the amount of mobile/less mobile polymer in each sample, but one needs to keep in mind that there is a (usually weak) signal decay during the echo time (true relaxation or imperfection effects), which needs to be accounted for. The general strategy is to fix as many as possible shape parameters (τ, b) of the individual components at predetermined values and then use them in a multicomponent fit to the FID signal, which is not subject to an intensity bias of the different components. Another point to mention is that we generally only fit MSE/FID data up to 0.25 ms since the decay at longer times is dominated by field inhomogeneities, the corresponding FID shape of which is not precisely known. The initial part is, however, generally well described by a simple modified exponential. Details on our curve-fitting strategy are described in ref 20.

Glass−Rubber Transition in PEA. We will first look at the MSE signals of the poly(ethyl acrylate) (PEA) matrix at various temperatures around and in particular above the glass transition. The calorimetric T_g of PEA is about 250 K.[32] However, glass transition effects on the NMR observables only set in several tens of K higher, i.e., when the segmental dynamics (α process) reaches correlation times of 0.1−0.01 ms, corresponding to the range where it is of the order of the inverse of the average dipolar coupling constant in the static limit. The MSE-refocused FIDs shown in Figure 2a reflect a typical motional-narrowing phenomenon in the mentioned temperature region, proving the influence of the glass−rubber transition. For a crude analysis, one can use the theory of Anderson and Weiss[33] to obtain an analytical (second-moment) approximation of a dipolar FID for a spin pair:

$$I_{\mathrm{FID}}(t) = \langle \cos \int_{\tau}^{t+\tau} \omega(\theta,\tau)\, \mathrm{d}\tau \rangle$$

$$= \exp\left[-M_2 {\tau_c}^2 \left(e^{-t/\tau_c} + \frac{t}{\tau_c} - 1 \right) \right] \qquad (2)$$

The dipolar frequency $\omega(\theta,\tau)$ is proportional to $D \times P_2(\cos\theta)$, and the latter is a random function in time, owing to the orientation fluctuations of the internuclear vector described by θ. For the simple case of isotropic rotational diffusion, for which the autocorrelation function of $P_2(\cos\theta)$ is a simple exponential $\sim\exp[-t/\tau_c]$, standard procedures[34] can be used to arrive at the above analytical result, where the second moment $M_2 \approx (9/20)D^2$ is related to the largest dipole−dipole pair couplings D in the system.

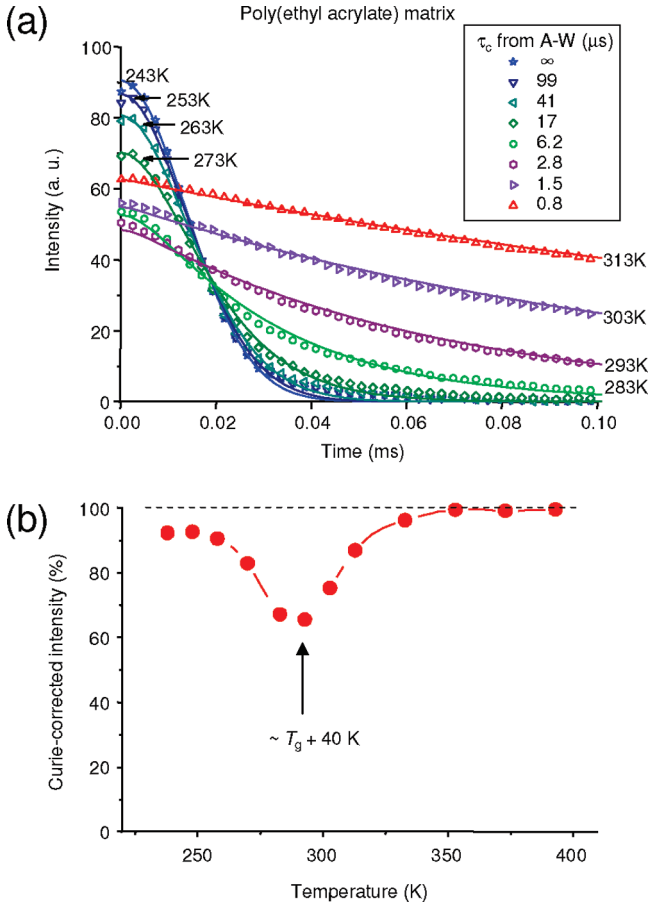

Figure 2. (a) MSE-refocused FID signals as a function of the acquisition time for a PEA matrix at various temperatures between 243 and 313 K (symbols), and results of fits to eq (2) (solid lines). The static second moment $M_2 \approx 5500\ \mathrm{ms}^{-2}$ was obtained by a fit with $\tau_c \to \infty$ to the FID at 243 K. (b) Initial intensity of the MSE-refocused FIDs plotted as a function of the temperature. The intensities have been corrected according to the Curie law. The minimum in the signal intensity at around $T_g + 40$ K is expected for an MSE experiment, the refocusing action of which is perturbed by molecular motion in the 10−100 kHz range.

Equation (eq 2) provides a good fit to the experimental data, with correlation times in the realistic range (Figure 2a). Note that the obtained τ_c is nontrivially related to a combination of main-chain segmental fluctuations (α process) as well as faster motions of the side-chains (β process). These are known to be coupled for the case of poly(alkyl methacrylates),[35] and similar complexity can be expected for PEA. A more complete analysis would of course have to embody a more complex form of the effective P_2 autocorrelation function, and one would also have to take into account that the high-temperature FIDs are already influenced by magnetic-field inhomogeneities or residual dipolar couplings related to cross-links. However, the general shape of the Anderson-Weiss function (eq 2) does not depend much on the specific form of the underlying correlation function, and is, over the whole τ_c range, well approximated by a simple modified exponential, $I_{\mathrm{FID}}(t) \sim \exp[-(t/\tau)^b]$, which justifies simple fitting approaches of the initial time range.

Figure 2b provides a second confirmation of the typical signature of a glass−rubber transition. We plot the variation of signal intensity after the MSE, which exhibits the typical minimum in the intensity at a few tens of Kelvin above the glass transition. This behavior is characteristic of an MSE, which is a full dipolar/chemical-shift echo. The formation of

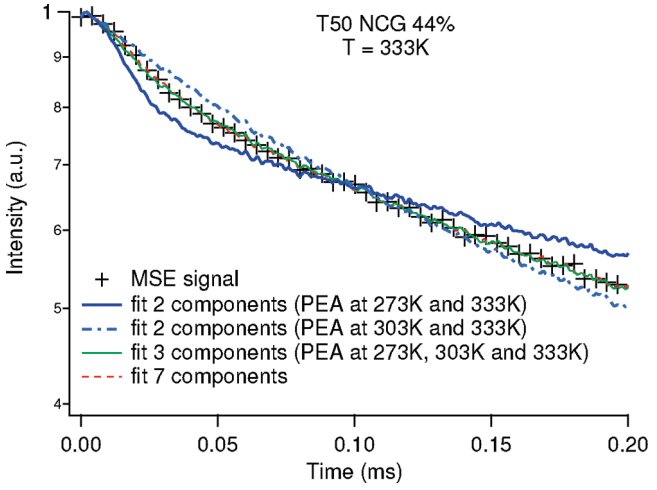

Figure 3. MSE signal as a function of the acquisition time for the T50 NCG 44% sample at 333 K fitted with different combinations of MSE signals of the PEA matrix between 253 and 333 K. We see that at least 3 components are needed to fit the experimental signal, in agreement with the presence of a gradient of polymer mobility.

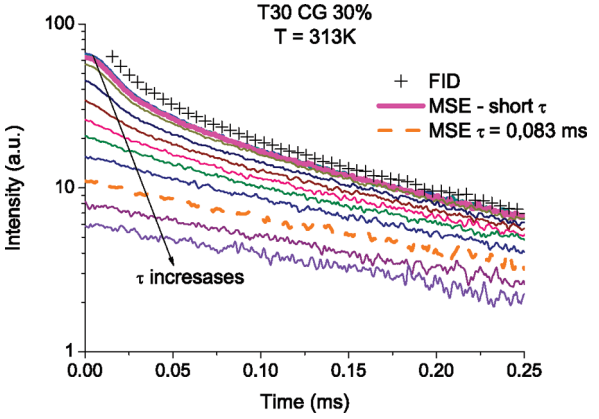

Figure 4. FID and MSE-FID signals as functions of the acquisition time for the sample T30 CG 30% at 313 K and for various τ_{MSE}. As τ_{MSE} increases, more and more of the initial fast decaying signal is lost. For $\tau_{MSE} \geq 0.083$ ms (that is below the dashed line), only the modified exponential signal remains and the parameters for the elastomer part can be determined: b_n and τ_n have here been determined on the curve corresponding to $\tau_{MSE} = 0.083$ ms. With MSE-FID curve at short τ_{MSE} (0.0126 ms for the thick line), the parameters for the "intermediate" and "glassy" parts are extracted: b_i, τ_i, and τ_g. Then, keeping all those parameters fixed, the FID is fitted in order to get the proportion of each component.

such an echo is only possible either in the slow- or the fast-motion limit, but is impeded when molecular motion takes place on the time scale of the refocused interaction (D^{-1}) and the echo (both $\sim$50 μs). The data demonstrate that in a more complex multicomponent sample with a distribution in T_g, the parts that exhibit dynamics in the intermediate motional regime may be underestimated by up to 40%. This is why our quantitative analysis below relies on unrefocused FID data.

Model Filled Elastomers. Existence of a Gradient of Mobility. As seen in the Introduction, a gradient of glass transition temperature is expected around the silica particles, which should lead to a gradient of polymer mobility in the filled elastomers. To check this in our samples, we measured MSE-refocused FIDs at a given temperature and fitted them with a linear combination of *experimental* MSE-FID signals of the pure PEA matrix at different temperatures (Figure 3, sample T50 NCG 44% at 333 K). We chose to use experimental data as base functions rather than analytical representations, noting that the fits in Figure 2a do not perfectly match the data.

We found that at least three components were needed to obtain an accurate representation. While a fit with seven components (PEA 253 K, 263 K, 273 K, 283 K, 293 K, 303 K, and 333 K) trivially matches the data extremely well, we note that with the three most significant components, PEA at 273 K—that is glassy, at 303 K—that is with an intermediate mobility, and at 333 K—that is at the experiment temperature, the fit is still very good. A combination of only two components is however never sufficient to describe the experimental signal. This means that at least three different kinds of polymer mobility are present in the filled elastomers. This observation is in agreement with the existence of a gradient of T_g around the solid particles (which cannot be described with a simplistic core−shell approximation at low temperature).

Determination of the Rigid Polymer Fraction. As we will see in the MQ experiment section, the CG samples contain a fraction of highly cross-linked polymer. We could then not use the MSE-FID signal of the PEA matrix (with 0.3 mol % of cross-linker, like the filled samples) to fit the MSE-FID signal of the CG samples. We thus decided to use an analytical fit composed of modified exponential functions, which can be applied to all the samples. We used three components, as two components were shown to not give a satisfactory fit for all the temperatures as we can see in Figure 5a. Reliable fitting was possible with all the parameters b and τ free except for the rigid (Gaussian) part where b_g was fixed to 2. The fitting function was thus

$$M(t) = M_0[a_g \exp(-(t/\tau_g)^{b_g}) + a_i \exp(-(t/\tau_i)^{b_i}) + a_n \exp(-(t/\tau_n)^{b_n})] \quad (3)$$

where g stands for glassy, i for intermediate and n for network.

The determination of the parameters was done using MSE-FID signals with different τ_{MSE} (see Figure 4). As τ_{MSE} increases (from 0.0126 to 0.123 ms), more and more of the solid signal is lost. From $\tau_{MSE} = 0.083$ ms (here), all the rigid signal is lost and the MSE-FID signal can be fitted with simply one modified exponential. This curve is thus used for the determination of the parameters b_n and τ_n, which will then be kept constant. The three other parameters are determined by fitting the MSE-FID signal with the shortest τ_{MSE}. This is done on three MSE-FID signals with a short τ_{MSE} and an average value of each parameter is taken.

For all the samples we found similar parameters: $b_n \simeq 1$, $b_i \simeq 1.3$, $\tau_g \simeq 0.02$ ms, $\tau_i \simeq 0.06$ to 0.1 ms, and $\tau_n \simeq 0.3$ to 1 ms depending on the temperature. A typical decomposition of the MSE-FID signal into three components is shown in Figure 5b. We can note here that τ_n is always smaller in the filled rubbers than in the matrix at the same temperature. The elastomer thus appears less mobile in the filled samples, which may simply be due to a higher effective cross-link density, as we will see in the MQ NMR section. However, the field inhomogeneity (shim limit and field distortions due to filler particles) may also play a role here, such that τ_n should not be overinterpreted. Simple Hahn−echo experiments could possibly yield better values, yet the MQ experiments are of course the route of choice for an in-depth characterization of the elastomer fraction.

Finally, keeping all those parameters fixed, we could fit the FID and find the fraction of each component a_g, a_i, a_n. In effect, even if the MSE-FID gives a well-refocused decay, there

is still a loss of intensity especially for polymer just above T_g (as we can see in Figure 2b). That is why, once the shape of the decay has been carefully fitted on the MSE-FID signals, we determine the amount of each component directly on the FID.

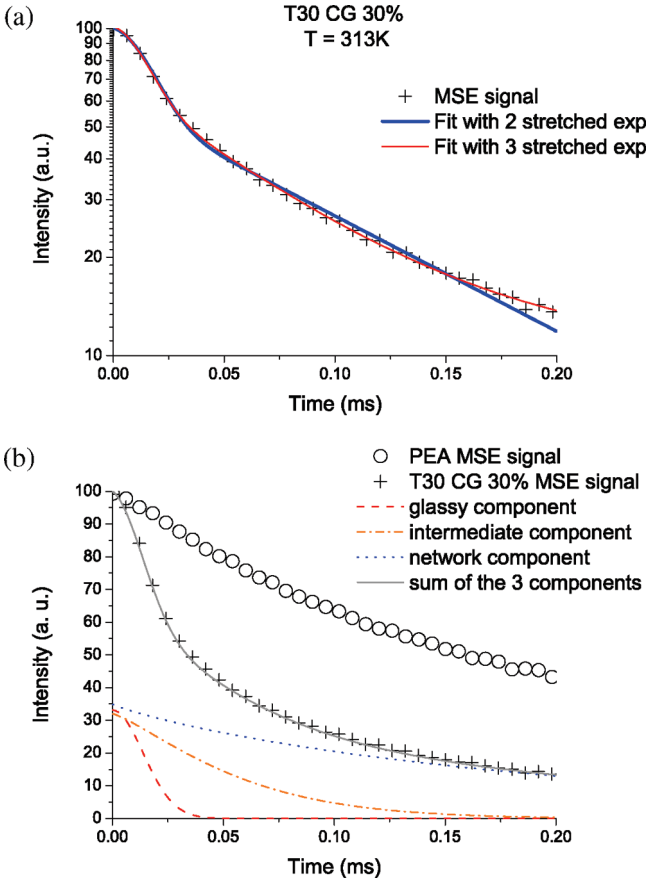

Figure 5. MSE-FID signal as a function of the acquisition time for the T30 CG 30% sample at 313 K fitted with the sum of 2 or 3 modified exponentials (a). Decomposition of the MSE-FID signal into 3 stretched exponentials (b).

This analysis is done on all the samples at 313, 333, 353, 373, and 393 K, that is between $\sim T_g + 40$ K and $T_g + 120$ K. Examples of the variation of each component with the temperature are given in Figure 6, parts a and c. We remark that the amount of "glassy" polymer does not vary much with the temperature and that for the CG samples, it is close to the fraction of protons coming from the grafters and ethoxy groups around the silica particles. This latter quantity can be estimated thanks to elemental analysis and is shown in Figure 6, parts a and c, as the shaded areas. For the NCG samples, however, the glassy fraction is slightly smaller that the amount of grafter and ethoxy. In effect, in this case the grafters are rather long chains (8 carbons), not covalently linked to the polymer. They can thus be more mobile than the polymer and not be included in the glassy fraction.

From now on, we call "immobilized" polymer the sum of the "glassy" and "intermediate" parts.

Solvent−Temperature Equivalence. At various solvent weight fractions, the amount of "glassy" and "intermediate" polymer was measured. The results obtained with toluene or dichloroethane were similar and the dichloroethane case is plotted in Figure 6, parts b and d, for one CG and one NCG sample. We see that the amount of rigid polymer decreases with the solvent content, similarly to what happens with an increase of the temperature. In effect, the addition of solvent induces a decrease in the glass transition temperature due to an increase in the configurationnal entropy of the polymer chains,[36] as shown in Figure 7a. This means that at constant temperature, the temperature difference $T - T_g$ is simply increased by swelling. We can show that solvent and temperature have exactly the same consequences on the polymer dynamics by plotting the amount of immobilized polymer as a function of $T - T_g$. We see in Figure 7 that we indeed obtain master curves.

Influence of the Silica Content and Diameter and of the Grafting Agent. The glassy and immobilized polymer fractions (a_g and a_g+a_i from eq (3)) have been measured for all the samples at various temperatures and the results are plotted at each temperature in Figure 8 as a function of the silica specific surface (total silica surface per volume unit, $3\Phi/R_{Si}$ in m^{-1}, R_{Si} being the mean silica radius and Φ the

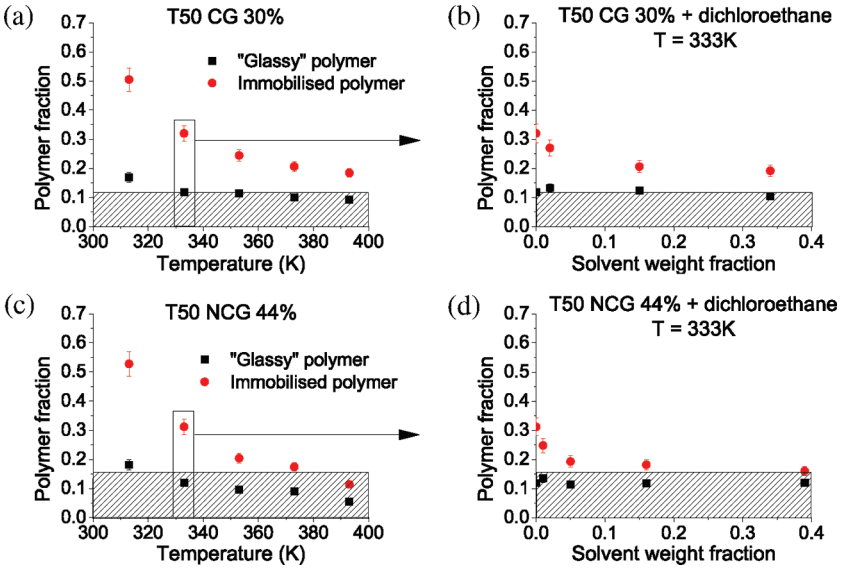

Figure 6. Evolution of the immobilized polymer fraction as a function of the temperature (a and c) and as a function of dichloroethane weight fraction (b and d). The shaded areas correspond to the fraction of protons coming from the grafters and ethoxy groups on the silica particles (from elemental analysis). The boxes and arrows simply highlight the fact that the solvent effect has been studied at 333 K, meaning that the first points (0% solvent) in the right figures correspond to the points in the boxes on the left figures.

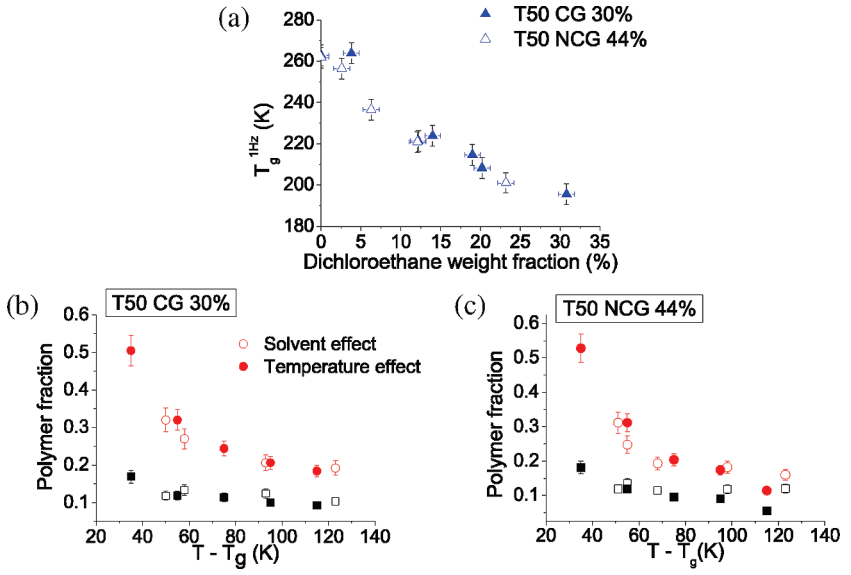

Figure 7. Glass transition temperature as a function of the solvent weight fraction (a). Glassy (squares) and immobilized (circles) polymer fraction as a function of $T - T_g$ for T50 CG 30% (b) and T50 NCG 44% (c). Temperature (filled markers) and solvent (open markers) have the same effect on the polymer mobility.

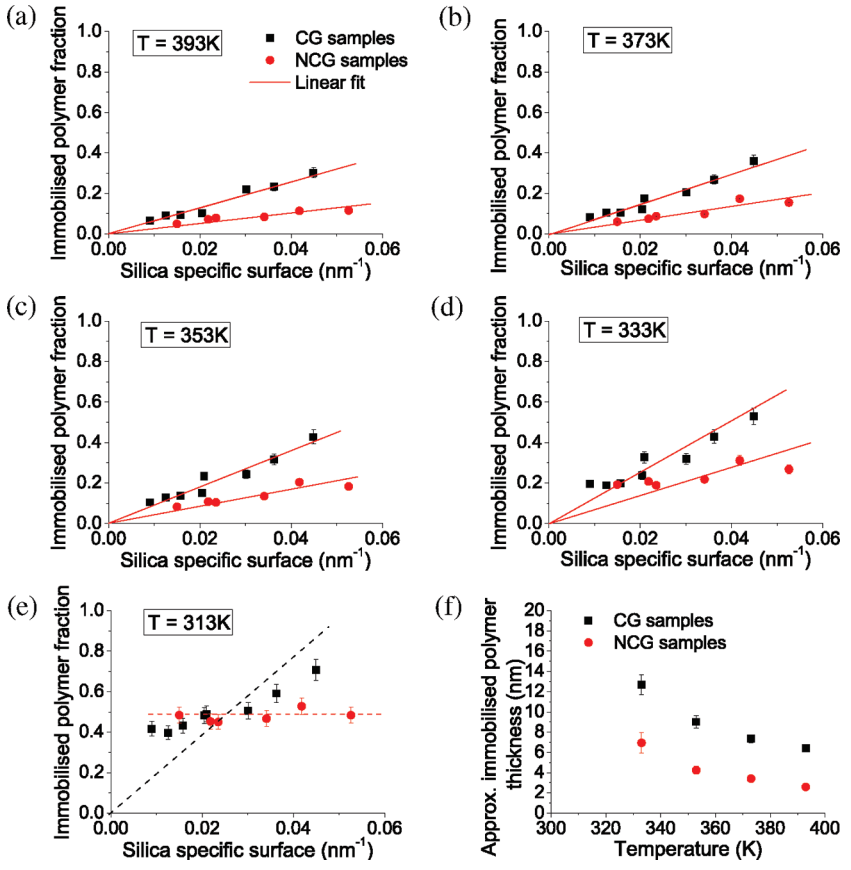

Figure 8. Fraction of immobilized polymer as a function of the silica specific surface at 393 (a), 373 (b), 353 (c), 333 (d), and 313 K (e). For each set of samples, a linear fit of the experimental points is shown. The slopes of those curves give an approximate thickness of immobilized polymer, which is plotted as a function of the temperature in part f. At 313 K, the temperature is too close to T_g, and the linear fit is not possible anymore.

silica volume fraction). The two sets of samples contain a fraction of immobilized polymer. Figure 8 shows that a covalent bond between the silica and the polymer matrix is not necessary to induce a gradient of T_g, an interaction—covalent or not—is sufficient. For the same silica specific surface, the NCG samples contain less immobilized polymer than the CG samples. This can be due to the different nature of the grafters - a stronger interaction in the case of covalent bonds which could lead to a larger range of interaction of the silica in the polymer network - but also to a different particles arrangement due to the different synthesis process used in each case (polymerization without solvent for the CG samples, with solvent for the NCG samples).

At 313 K, the interpretation of the plot is not clear and all the samples seem to show similar amounts of immobilized polymer. This is due to the fact that the temperature is too close to T_g, so that the FID decay shape of the PEA matrix cannot be separated well any more from the even more rigid surface material and the fits become ambiguous. The MSE-FID of pure PEA at 313 K in Figure 2a can in fact be fitted not only with either the given Anderson−Weiss function or a compressed exponential ($b > 1$) but also with a linear combination of a pure Gaussian and a pure exponential. The amount of immobilized polymer obtained at 313 K is thus not only the polymer whose dynamics is modified by the proximity of the silica surface but it contains also part of the elastomer fraction approaching its glass transition.

Another important feature is that at high enough temperature (333−393 K), the rigid polymer fraction is proportional to the silica specfic surface, so that the slope of the linear fit gives an approximate thickness of rigid polymer around the silica particles (Figure 8f). In fact, two effects compensate each other: this approximate thickness is overestimated because we do not take into account the curvature of the silica particles, but it is also underestimated because it also misses the overlap effect when the particles are in average closer than the rigid thickness.

Cross-Linking Inhomogeneities: MQ NMR Measurements. MQ experiments give an insight into the orientation of the polymer segments in the network and thus on the topological constraints like cross-links and entanglements. We will first see the effect of a change in cross-link density in a PEA matrix on the DQ build-up curves and then see that the two sets of filled samples show very different responses.

PEA Matrix. First, the DQ build-up curves of PEA matrix with different cross-link densities are shown in Figure 9. Since the residual dipolar couplings are the origin of the appearance of a DQ signal build-up and their strength is directly proportional to the cross-link density, it is clear that a higher cross-link density results in a time scaling of the DQ build-up curve in cases where the microstructure (homogeneity) of the networks is similar. If we take the PEA matrix with 0.3 mol % of cross-linker as the reference (that is the same quantity of cross-linker as used for the filled samples), we can fit the higher cross-linked PEA matrix by simply scaling this curve along the time axis (corresponding to an additive shift on a logarithmic scale). In the inset, we confirm that the scaling factor used depends linearly on the cross-linker concentration used in the synthesis. Note that we could in this case not use an analytical fit of the DQ build-up curves, as done in previous publications[22,24] because of the inhomogeneous behavior of the PEA matrix due to its side chains ("spin system inhomogeneity"). A similar yet less serious complexity of the experimental response is for instance exhibited by styrene−butadiene−rubber with its different monomer units and the pending phenyl group, as discussed in ref 24.

Model Filled Elastomers. Glassy Fraction: Necessity of a MAPE Filter. The DQ experiments are performed at 393 K, where the rigid polymer fraction is the lowest. However, this rigid polymer exhibits strong dipolar couplings, and we have to suppress its (weak) contribution to the DQ signal in order to study only the changes of the elastomer fraction. For that, we place a MAPE dipolar filter − similar to the MSE we used previously—before the DQ sequence. Increasing the filter length τ_{MAPE} leads to a rapid decrease in the Gaussian part of the signal until the response becomes more or less singly exponential (see Figure 10). For the sample with the largest rigid fraction (T30 CG 30%), we see that at $\tau_{MAPE} = 0.164$ ms only the elastomer response is present. The value of τ_{MAPE} was kept constant for all the filled samples and the DQ study will thus be limited to the elastomer part of the filled samples. It was checked that this filter had no influence on the DQ build-up curves of the PEA matrix.

As expected, the temperature also had no influence on the DQ build-up curves of the pure matrix networks, which is due to the normalization process explained in the Samples and Experimental Techniques. However, this is not the case for the filled samples. In effect, changing the temperature leads to a change in the amount of immobilized polymer and thus in the quantity of signal suppressed by the MAPE filter so that τ_{MAPE} would have to be adjusted to each temperature, in all cases with the criterion that the signal exhibits only one component. Here we will restrict our study to a fixed temperature of 393 K.

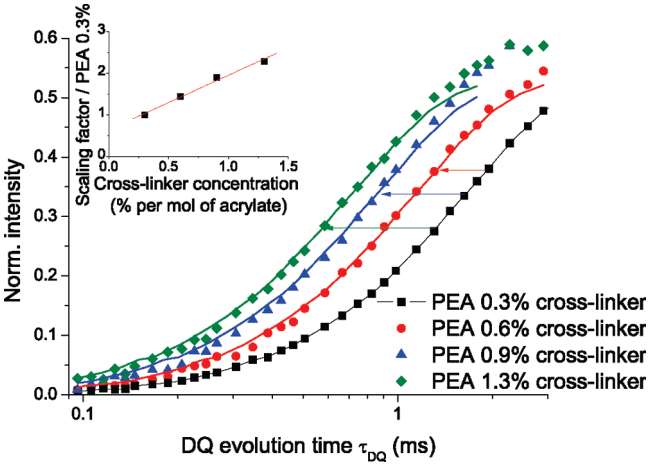

Figure 9. DQ build-up curves for PEA matrix with various cross-link density ($T = 393$ K). In the inset, the scaling factor applied to the reference PEA 0.3 mol % cross-linker curve to superpose it to the curve of the PEA matrix with a higher cross-link density. A higher cross-link density is thus seen as a shift (scaling on a linear scale) of the DQ build-up curve to the shorter times.

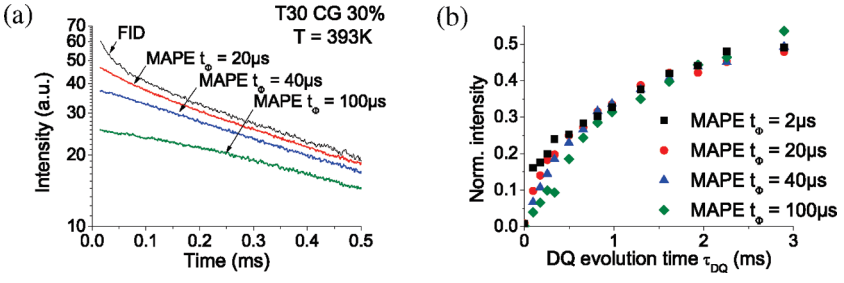

Figure 10. Adjustment of the MAPE filter. As t_ϕ is increased in the MAPE filter, the solid-like response in the FID response (as a function of the acquisition time) decreases (a). The filter time chosen is $t_\phi = 40\mu s$, which corresponds to pure elastomer response. The corresponding DQ build-up curves are presented in part b.

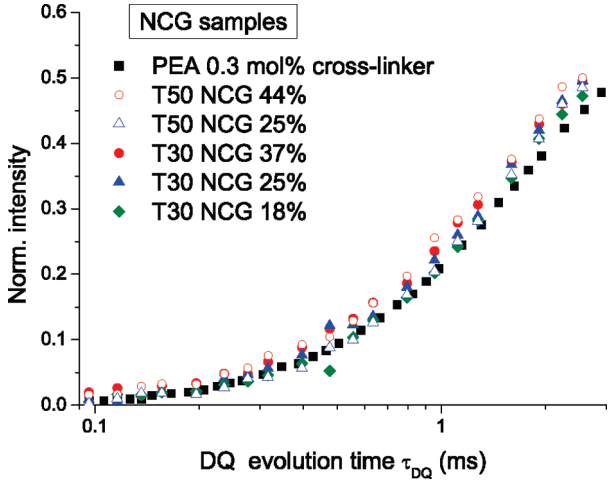

Figure 11. DQ build-up curves of the NCG samples. These can be fitted by the curve of the reference PEA matrix slightly shifted (time-scaled). The NCG samples are thus homogeneously cross-linked with an effective cross-linker concentration slightly above 0.3 mol %.

NCG samples Are Homogeneously Cross-Linked Whereas CG Samples Show a Fraction of Highly Cross-Linked Polymer. Figure 11 shows the DQ build-up curves of the NCG samples, compared with the reference PEA matrix. It shows that all the curves can be fitted with the slightly time-scaled (shifted) reference curve. It means that the elastomer part of the NCG samples is homogeneously cross-linked with an effective cross-linked density slightly above 0.3 mol % cross-linker.

The behavior of the CG samples is very different (see Figure 12). In this case, the DQ build-up curves are not superimposed on the reference and are shifted to shorter DQ evolution time, meaning that they are more cross-linked than expected. The DQ build-up curves could not be fitted with only the time-scaled DQ build-up curve of the PEA matrix, which means that the samples are not only more highly cross-linked, but also that they are not homogeneous. We can model the response of the CG samples by a sum of two pure-matrix components, time-scaled to a different degree. This shows that the use of a grafting agent like TPM creating covalent bonds between the silica particles and the matrix has an influence on the cross-link density around the silica particles. This is an observation that was not made in any conventional filled elastomer system.[24] We attribute this to the good particle dispersion, the homogeneous surface grafting density, and the consequently large volume fraction of affected material.

An attempt of quantification of the amount of polymer with a higher cross-link density has been made, however, we need to keep in mind that, due to the MAPE filter, we are probing only *part* of the polymer and that it is dependent on the τ_{MAPE} chosen. Although we set τ_{MAPE} such that mostly the glassy part of the signal was suppressed, we of course have to consider that there is a smooth gradient in T_g, which is likely coupled to an inhomogeneity on the effective cross-link density.

For the fits, the scaling factors obtained were around 1.2 for the main component and ranged between 5 and 10 but with a rather high uncertainty for the other component. We thus decided to fix the second scaling factor to 7.5 (which effectively corresponds approximately to 5 mol % of cross-linker, see Figure 2b) and keep only two parameters free: the shift factor of the main fraction of the elastomer and the quantity of polymer with a higher cross-link density. The results are representative only of the elastomer fraction of each sample, but it can be expected that rigid (glassy) polymer located close to the silica particles has an even higher effective cross-link density. The total amount of highly cross-linked polymer would thus be the sum of the immobilized polymer fraction (determined by MSE-FID at 393 K) and the fraction of elastomer with a higher cross-link density extracted from the fits. This quantity is obviously linked to the silica specific surface (see Figure 13).

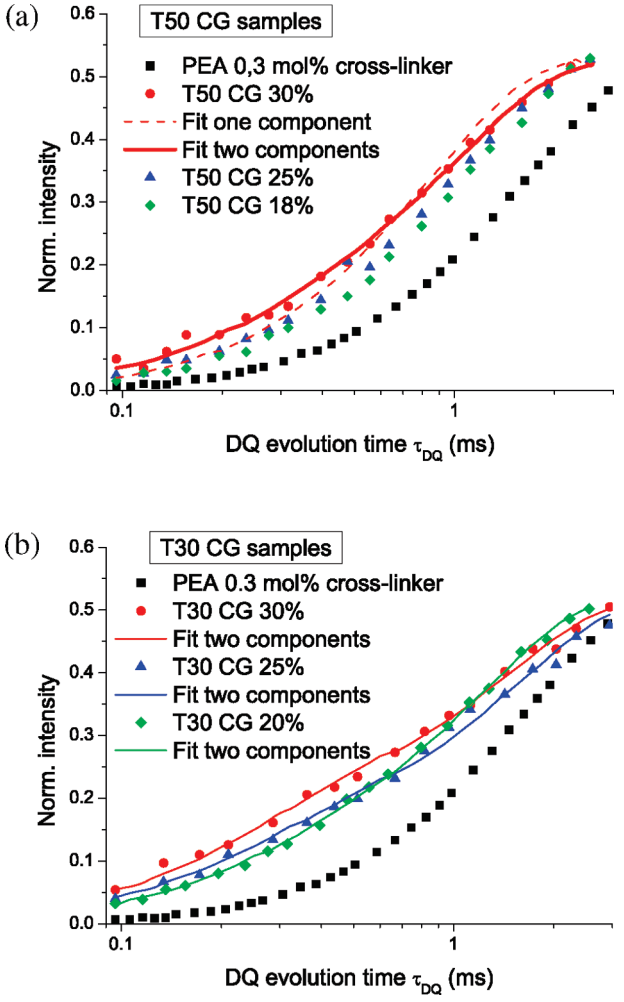

Figure 12. DQ build-up curves of the CG samples. They are not superimposed on the one of the reference PEA matrix, meaning that the CG samples appear more cross-linked than the polymer matrix with the same amount of cross-linker introduced (0.3 mol % to the monomer). In part a, the DQ build-up curve of the T50 CG 30% sample cannot be fitted with only one time-shifted PEA curve (thin line), we need to use a combination of two time-scaled PEA curves (thick line), meaning that the sample is heterogeneously cross-linked.

Discussion and Conclusion

In this study of model filled elastomers, we showed through MSE-FID NMR experiments the existence of a fraction of immobilized polymer and more precisely of at least three kinds of polymer mobility. This is in agreement with the existence of a *gradient* of polymer mobility, which can be interpreted as a gradient of glass transition temperature in the vicinity of the solid particles, as it has been shown for thin polymer films deposited on a substrate and interacting through hydrogen bonds.[11] An increase in the temperature or the addition of solvent both induce a decrease in the immobilized polymer fraction. In effect, in both cases $T - T_g$ is increased, either by increasing T or by decreasing T_g, and thus the polymer mobility is increased.

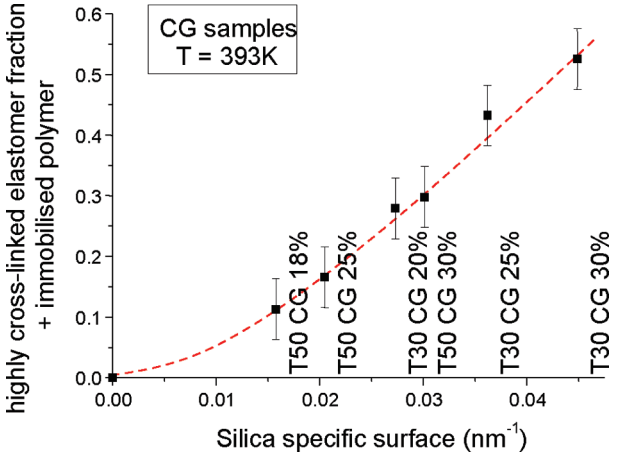

Figure 13. Amount of highly cross-linked polymer plus immobilized polymer at 393 K plotted as a function of the silica specific surface (scaling factor fixed to 7.5). The line is a guide for the eye.

The effect of the coupling agent has also been investigated. Whether the grafter creates a covalent bond between the filler or not does not change the overall behavior: in both cases there is a gradient of mobility, even if the amount of immobilized polymer is slightly less when the interaction between the filler and the polymer is not covalent.

MQ NMR experiments then pointed out the presence of a fraction of highly cross-linked polymer in the case of the covalently grafted samples but not for the noncovalently grafted samples. The presence of a highly cross-linked polymer fraction had not been previously detected in conventional systems and is most likely the result of the good particle dispersion in our model samples. It remains to be investigated in how far this effect is relevant for the reinforcement mechanisms in conventional (aggregated) filled elastomers, where the fraction of polymer in the vicinity of the fillers is obviously much smaller.

From those observations we can finally conclude that a connection—i.e., a covalent bond or a strong adsorption (as in the system PDMS−silica[37])—between the filler and the polymer is not a necessary prerequisite for the existence of a gradient of T_g, even if it is probably responsible for a highly cross-linked polymer fraction. This indicates that the gradient of glass transition temperature is related more to the presence of an *interaction* between the fillers and the polymer than to a *connection* between them.

References and Notes

(1) Wang, M. *Rubber Chem. Technol.* **1998**, *71*, 520–589.
(2) Chazeau, L.; Brown, J.; Yanyo, L.; Sternstein, S. *Polym. Compos.* **2000**, *21*, 202–222.
(3) Heinrich, G.; Kluppel, M. *Filled Elastomers Drug Deliv. Syst.* **2002**, *160*, 1–44.
(4) Kluppel, M. *Filler-Reinforced Elastomers/Scanning Force Microscopy*; Advances in Polymer Science, Springer Verlag: Berlin, Heidelberg, 2003, Vol. 164/2003, 1−86.
(5) Kaufman, S.; Slichter, W.; Davis, D. *J. Polym. Sc., Part A-2: Polym. Phys.* **1971**, *9*, 829.
(6) Kenny, J.; McBrierty, V.; Rigbi, Z.; Douglass, D. *Macromolecules* **1991**, *24*, 436–443.
(7) Ou, Y.; Yu, Z.; Vidal, A.; Donnet, J. *J. Appl. Polym. Sci.* **1996**, *59*, 1321–1328.
(8) Litvinov, V.; Steeman, P. *Macromolecules* **1999**, *32*, 8476–8490.
(9) ten Brinke, J.; Litvinov, V.; Wijnhoven, J.; Noordermeer, J. *Macromolecules* **2002**, *35*, 10026–10037.
(10) Leu, G.; Liu, Y.; Werstler, D.; Cory, D. *Macromolecules* **2004**, *37*, 6883–6891.
(11) Fryer, D.; Peters, R.; Kim, E.; Tomaszewski, J.; de Pablo, J.; Nealey, P.; White, C.; Wu, W. *Macromolecules* **2001**, *34*, 5627–5634.
(12) Long, D.; Lequeux, F. *Eur. Phys. J. E* **2001**, *4*, 371–387.
(13) Berriot, J.; Montes, H.; Lequeux, F.; Long, D.; Sotta, P. *Macromolecules* **2002**, *35*, 9756–9762.
(14) Berriot, J.; Lequeux, F.; Monnerie, L.; Montes, H.; Long, D.; Sotta, P. *Journal of Non- Crystalline Solids* **2002**, *307−310*, 719–724.
(15) Berriot, J.; Montes, H.; Lequeux, F.; Long, D.; Sotta, P. *Europhys. Lett.* **2003**, *64*, 50–56.
(16) Montes, H.; Lequeux, F.; Berriot, J. *Macromolecules* **2003**, *36*, 8107–8118.
(17) Saalwächter, K.; Kluppel, M.; Luo, H.; Schneider, H. *Appl. Magn. Reson.* **2004**, *27*, 401–417.
(18) Saalwächter, K. *Macromolecules* **2005**, *38*, 1508–1512.
(19) Maus, A.; Hertlein, C.; Saalwächter, K. *Macromol. Chem. Phys.* **2006**, *207*, 1150–1158.
(20) Mauri, M.; Thomann, Y.; Schneider, H.; Saalwächter, K. *Solid State Nucl. Magn. Reson.* **2008**, *34*, 125–141.
(21) Saalwächter, K. *J. Am. Chem. Soc.* **2003**, *125*, 14684–14685.
(22) Saalwächter, K.; Herrero, B.; Lopez-Manchado, M. A. *Macromolecules* **2005**, *38*, 9650–9660.
(23) Saalwächter, K. *Prog. Nucl. Magn. Reson. Spectrosc.* **2007**, *51*, 1–35.
(24) Valentin, J.; Posadas, P.; Fernandez-Torres, A.; Malmierca, M.; Gonzalez, L.; Chassé, W.; Saalwächter, K. *Macromolecules* **2010**, *43*, 4210–4222.
(25) Berriot, J.; Martin, F.; Montes, H.; Monnerie, L.; Sotta, P. *Polymer* **2003**, *44*, 1437–1447.
(26) Berriot, J.; Montes, H.; Martin, F.; Mauger, M.; Pyckhout-Hintzen, W.; Meier, G.; Frielinghaus, H. *Polymer* **2003**, *44*, 4909–4919.
(27) Stöber, W.; Fink, A.; Bohn, E. *J. Colloid Interface Sci.* **1968**, *26*, 62–69.
(28) Sunkara, H.; Jethmalani, J.; Ford, W. *Chem. Mater.* **1994**, *6*, 362–364.
(29) Jethmalani, J.; Ford, W. *Chem. Mater.* **1996**, *8*, 2138–2146.
(30) Jethmalani, J.; Ford, W.; Beaucage, G. *Langmuir* **1997**, *13*, 3338–3344.
(31) Jethmalani, J.; Sunkara, H.; Ford, W.; Willoughby, S.; Ackerson, B. *Langmuir* **1997**, *13*, 2633–2639.
(32) Bandrup, J.; Immergut, E. H.; Grulke, E. A. *Polymer Handbook*; John Wiley & Sons: New York, 1999.
(33) Anderson, P. W.; Weiss, P. R. *Rev. Mod. Phys.* **1953**, *25*, 269–276.
(34) Kimmich, R. *NMR Tomography, Diffusometry, Relaxometry*; Springer: Berlin, 1997.
(35) Wind, M.; Graf, R.; Heuer, A.; Spiess, H. W. *Phys. Rev. Lett.* **2003**, *91*, 155702.
(36) Chow, T. *Macromolecules* **1980**, *13*, 362–364.
(37) Şerbescu, A.; Saalwächter, K. *Polymer* **2009**, *50*, 5434–5442.